

Opportunistic Group Antenna Selection in Spatial Modulation Systems

Yuanyuan He¹, Member, IEEE, Saman Atapattu², Member, IEEE, Chintha Tellambura³, Fellow, IEEE, and Jamie S. Evans⁴, Senior Member, IEEE

Abstract—This paper proposes an opportunistic spatial modulation (OSM) scheme where the transmit antennas are divided into $K \geq 1$ equal groups, and the best antenna from each group is selected to form a K transmit antenna subset for implementing spatial modulation (SM). Thus, the activation of one antenna from the subset to transmit one of the M -ary modulation symbols achieves a data rate of $\log_2(K) + \log_2(M)$ bits per channel use. Notably, special cases of OSM include conventional SM and pure single transmit antenna selection. To characterize and comparatively evaluate OSM, we first consider phase-shift keying modulation and derive a closed-form, improved union-bound of symbol error probability (SEP) with a single-antenna receiver. Explicit expressions for the SEP in the high signal-to-noise ratio regime are also presented. Extensions to quadrature amplitude modulation analysis and simulations of multiple-antenna reception case are also provided. Simulation results corroborate the analytical results and reveal the interesting interplay between the signal and spatial constellation diagrams. For a given number of transmit antennas and targeted data rate, asymptotically, the SEP can be minimized by using only one antenna group and the largest size of signal constellation, as this configuration achieves the full-diversity order.

Index Terms—Antenna selection, spatial modulation, multiple-input single-output, symbol error probability, diversity gain.

I. INTRODUCTION

Spatial Modulation (SM) is a promising single radio-frequency (RF) multiple-antenna transmission technique, to overcome some drawbacks of conventional multiple-input multiple-output (MIMO). These include inter-antenna synchronization (IAS), inter-channel interference (ICI), high complexity and high energy consumption, which increases with the growth in the number of antennas/RF chains [1], [2]. Fundamentally, SM activates only one of multiple transmit antennas during each channel-use (i.e., only single RF chain

is needed), but it achieves higher spectral efficiency (SE) than conventional single-antenna transmission by embedding extra data symbols into activated transmit antenna indexes [2]. Consequently, the SM transmit signal has three dimensions - namely antenna-index modulation and the conventional 2D signal modulation. At the receiver side, the advantage of zero ICI allows single-stream based maximum-likelihood (ML) decoding, but its complexity does not grow exponentially with the size of the signal set [3], [4]. Thus, by incorporating numerous/large-scale passive transmit antenna elements without requiring extra RF chains, SM-MIMO offers excellent SE as large as that of the conventional high-complexity and energy-hungry MIMO. Moreover, tens/hundreds of antennas can be compactly packed at both transmitter and receiver using emerging mmWave technologies [5]. The applications of SM to mmWave channels have been investigated in [6]–[8]. In [9], the performance of SM is validated for the first time via an experimental testbed, and [10] provides a general survey of the SM design framework as well as of its intrinsic limits. In [11], the energy efficiency (EE) of SM is evaluated at multi-antenna base stations. These features clearly accentuate the inherent potential of SM-MIMO as an attractive low-complexity and EE option for the next generation wireless applications.

A. Related Work

SM is an open-loop scheme that does not require channel state information at the transmitter (CSIT). This is because the activated transmitter antenna is directly determined by the spatially modulated information bit sequence [12]. However, deep fading of the active antenna channel may dramatically increase bit errors. Closed-loop SM schemes have shown to be effective approaches to alleviate this problem by exploiting some form of CSIT. One such scheme is transmit antenna subset selection-aided SM (TASS-SM), where antenna subsets are selected for SM use instead of all the transmit antennas [13]–[26]. In [13], three TASS schemes are proposed for a space-shift keying (SSK)-MIMO system (SSK is a special case of SM, where only the antenna indices convey information): i) largest channel gain based TASS (LCGAS); ii) maximum of the difference between channels based TASS; and iii) a hybrid version of i) and ii). A capacity optimized TASS scheme called COAS (similar to LCGAS), is introduced for SM-MIMO in [14]. Although lacking transmit-diversity, it may nevertheless provides higher coding gain than conventional SM. An antenna correlation based TASS is examined in [15], which measures antenna difference using the cosine similarity.

Manuscript received December 22, 2017; revised May 6, 2018; accepted June 14, 2018. Date of publication June 29, 2018; date of current version November 16, 2018. This work is supported by the Australian Research Council (ARC) Discovery Project DP140101050, in part by the Melbourne School of Engineering of the University of Melbourne's Early Career Researcher Grant, and in part by the ARC Discovery Early Career Researcher (DECRA) Award DE160100020. The associate editor coordinating the review of this paper and approving it for publication was M. Di Renzo. (Corresponding author: Yuanyuan He.)

Y. He, S. Atapattu, and J. S. Evans are with the Department of Electrical and Electronic Engineering, The University of Melbourne, Parkville, VIC 3010, Australia (e-mail: yuhe@unimelb.edu.au; saman.atapattu@unimelb.edu.au; jse@unimelb.edu.au).

C. Tellambura is with the Department of Electrical and Computer Engineering, University of Alberta, Edmonton, AB T6G 1H9, Canada (e-mail: ct4@ualberta.ca).

Color versions of one or more of the figures in this paper are available online at <http://ieeexplore.ieee.org>.

Digital Object Identifier 10.1109/TCOMM.2018.2851567

A Euclidean distance (ED) optimized based TASS scheme called EDAS, is first proposed by [14]. By maximizing the minimum ED of the received SM constellation, it can achieve high transmit diversity gains [16]. Nevertheless, these gains are achieved at the cost of high computational complexity, requiring exhaustive search over all the possible antenna subsets.

Subsequently, several recent works have focused on reduced-complexity EDAS-SM schemes, via either decreasing the complexity of evaluating ED [14], [17], [18], [23] or lessening the search burden [15], [19]–[22], [24], at the expense of performance. Moreover, a more practical EDAS-SM scheme is studied by considering an error-infested feedback channel [25]. In [26], a joint transmit and receive antenna subset/codebook selection is proposed for feedback assisted full-duplex SM-MIMO. For existing TASS-SM schemes, rigorous performance analysis frameworks are difficult to develop. For example, although COAS-SM is one of the simplest TASS-SM schemes, its error rate or diversity order analysis is very limited [14]. Transmit pre-coding (TPC) aided SM (TPC-SM) is another promising closed-loop approach to augment SM performance. In [27], it is shown that TPC based on directly minimizing the bit error ratio (BER) surpasses that of maximizing the minimum ED. This work [28] also summarized several attractive TPC schemes for single-carrier (SC)-SM based large-scale MIMO multiuser downlink transmission systems. However, TPC-SM requires more detailed CSI (not just antenna indexes) at the transmitter, which maybe hard to realize in practice.

B. Summary of Contributions

In this paper, we propose a novel and tractable low-complexity TASS-SM scheme, called *opportunistic spatial modulation (OSM)*, where total N_t transmit antennas are divided into $K \geq 1$ equal groups, and the best antenna from each group is selected to form a new spatial constellation diagram for implementing SM. The activation one of the selected K antennas and the use of M -ary digital modulation achieves a data throughput of $\log_2 K + \log_2 M$ bits per channel use. The CSIT requirement of OSM is modest – just $K \log_2 \frac{N_t}{K}$ feedback bits from the receiver to the transmitter, which increases suitability for practical implementation. Moreover, the independent antenna grouping enables the development of comprehensive performance analysis of OSM. Our analysis also opens up a new avenue for future design of tractable TASS-SM with both low-complexity and high diversity order.

Note that, because this is the first such OSM scheme, we focus on the detailed performance analysis. To this end, we consider OSM with single-antenna receiver only (i.e., OSM-MISO), which is practically important due to the use of billions of single-antenna, pocket-sized handsets. Moreover, if we consider multiple-antenna reception, there are many options – such as maximal ratio combining, selection combining and others. However, analyzing them is beyond the scope of this paper and left as a future research topic. Nevertheless, we provide simulation results of OSM with multiple-antenna reception (OSM-MIMO). Both phase-shift keying (PSK) modulation and quadrature amplitude modulation (QAM) are considered. PSK is more suitable for

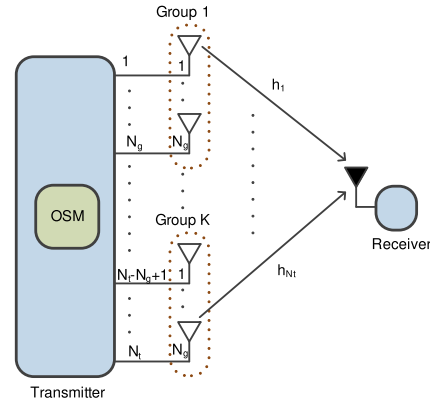


Fig. 1. The OSM-MISO system model.

EE applications [29]. Thus, Section III main results deal with PSK, and then we briefly highlight the extension to the QAM case in Section III-D.

Based on the proposed OSM (Fig. 1), this paper provides following technical contributions.

- 1) A rigorous derivation of explicit expressions for average symbol error probability (SEP) of OSM-MISO, based on a tightened union bound, is provided. Such bounds are difficult or non-existent for most existing TASS-SM schemes.
- 2) By systematically exploring asymptotic and diversity analysis of OSM-MISO, closed-form formulas for the asymptotic SEP of OSM-MISO are derived for the high SNR regime, and some interesting fundamental performance trends are also clearly identified.
- 3) In high SNR, we show that for a given number of transmit antennas and a target data throughput, the SEP can be minimized by using the fewest antenna groups and the highest possible signal constellation size, as this combination achieves the full-diversity order.
- 4) The performance and complexity of OSM-MISO are then compared with two well known TASS-SM schemes, namely COAS-SM and EDAS-SM. We find that OSM-MISO offers reduced CSI feedback overhead and low computational complexity, provides better error performance than COAS-SM as SNR increases. When compared to EDAS-SM, OSM-MISO displays a useful performance-complexity trade-off.
- 5) Extensions to QAM analysis and simulations of OSM-MIMO are also provided.

The remainder of the paper is organized as follows. Section II describes our proposed OSM-MISO. Section III analyzes its SEP. Section IV provides numerical and simulation results. Section V discusses the conclusions.

II. OPPORTUNISTIC SPATIAL MODULATION MISO (OSM-MISO)

This section describes the system model and the analytical model.

A. System Model

The OSM-MISO system (Fig.1) consists of a transmitter with N_t antennas and a single antenna receiver.

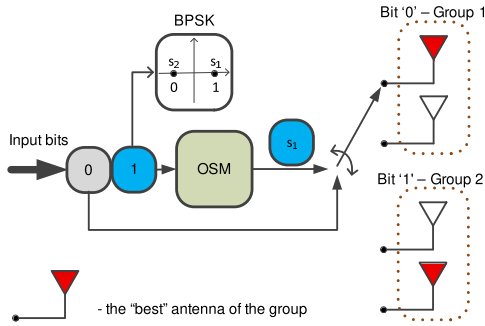


Fig. 2. The OSM bit-to-symbol mapping rule for $N_t = 4, K = 2$, BPSK.

M -ary signal amplitude/phase modulation (APM) with $M \geq 2$ is considered, which is comprised of symbols $\{s_1, \dots, s_M\}$ with each symbol s_m satisfying the unit-energy constraint i.e., $\mathbb{E}[|s_m|^2] = 1, \forall m = 1, \dots, M$. We assume that both $\log_2 N_t$ and $\log_2 M$ are positive integers. The MISO channel is denoted by $\mathbf{h} = [h_1, \dots, h_j, \dots, h_{N_t}] \in \mathbb{C}^{1 \times N_t}$, where h_j is the channel coefficient between the j th transmit antenna and the receiver, and all $h_j, j = 1, \dots, N_t$ are independent and identically distributed (iid) zero-mean and unit-variance complex Gaussians, i.e., $h_j \sim \mathcal{CN}(0, 1)$ (Rayleigh fading).

The novel feature of OSM is the opportunistic transmit antenna selection from groups of antennas followed by conventional SM. That is, the OSM scheme follows two steps: i) the antenna selection, and ii) the conventional SM implementation.

- Step I: The N_t transmit antennas are equally split into K groups, where $\log_2 K$ is an integer. Each group has $N_g = \frac{N_t}{K}$ antennas. The best antenna in each group, which is the one with the largest channel gain, is selected. For the k -th group, the selected antenna index and its channel coefficient are represented by $N_{(k)}$ and $g_{(k)}$, respectively, given as $N_{(k)} = \arg \max_{i \in [(k-1)N_g + 1, kN_g]} |h_i|$ and $|g_{(k)}| = \max_{i \in [(k-1)N_g + 1, kN_g]} |h_i|$. Then, the selected set of antenna indices and the corresponding set of channels are $\{N_{(1)}, \dots, N_{(K)}\}$ and $\{g_{(1)}, \dots, g_{(K)}\}$, respectively.
- Step II: The conventional SM technique is implemented based on the new ‘spatial constellation’, i.e., the set of antenna indexes $\{N_{(1)}, \dots, N_{(K)}\}$ and the ‘signal constellation’ of M -ary APM symbols set $\{s_1, \dots, s_M\}$.

Thus for OSM, the total number of bits per channel use (bpcu) is given by $B = \log_2(K) + \log_2(M)$ bpcu, where the $\log_2(K)$ bits choose a unique antenna index from $\{N_{(1)}, \dots, N_{(K)}\}$, and the other $\log_2(M)$ bits choose an APM symbol from $\{s_1, \dots, s_M\}$. Only one of the K selected antennas is activated for transmitting the mapped APM symbol while all other antennas remain inactive. An OSM example is given below.

Example 1: The OSM mapping principle is shown in Fig. 2 for $N_t = 4, K = 2$ and binary PSK (BPSK) case. The bit throughput $B = \log_2(2) + \log_2(2) = 2$ bpcu, where one bit is encoded by the antenna group indices (“0” for Group 1 and “1” for Group 2), and the other bit is encoded by BPSK symbols (“1” for $s_1 = +1$ and “0” for $s_2 = -1$). E.g., binary input ‘01’ activates the first antenna (which is the ‘best’ antenna of Group 1) to emit $s_1 = +1$.

The antenna selection and the OSM mapping rules are assumed to be known by both the transmitter and receiver a priori. However, only limited CSIT is needed because the receiver can estimate the full CSI, selects the K antennas and sends their indexes $\{N_{(1)}, \dots, N_{(K)}\}$ to the transmitter via an error-free and zero-delay feedback link [18].

Remark 1: OSM-MISO includes two conventional schemes as special cases: (1) when $K = N_t$, it becomes conventional SM-MISO; (2) when $K = 1$, it becomes conventional MISO with the ‘best’ single transmit antenna selection (TAS-MISO).

B. Analytical Model

At each transmission, only one transmit antenna will be active. Without loss of generality, the transmission of Group k with symbol s_m is elaborated here. Thus, the transmit signal can be expressed as $\mathbf{x}_{k,m} = \mathbf{A}\Upsilon_k s_m$, where $\mathbf{x}_{k,m} \in \mathbb{C}^{N_t \times 1}$; $\mathbf{A} \in \mathbb{C}^{N_t \times N_t}$ is a diagonal matrix $\mathbf{A} = \text{diag}(a_1, \dots, a_{N_t})$, with $a_i = 1$ if the i -th antenna is selected as the ‘best’ antenna in one of antenna groups, i.e. $i \in \{N_{(1)}, \dots, N_{(K)}\}$, otherwise $a_i = 0$; $\Upsilon_k \in \mathbb{C}^{N_t \times 1}$ indicates that the antenna Group k is chosen by first $\log_2(K)$ information bits, which is given as

$$\Upsilon_k \triangleq \underbrace{[0 \dots 0 \ 1 \dots 1 \ 0 \dots 0]^T}_{\text{From } (k-1)N_g + 1 \text{ to } kN_g \text{ entries are "1"}}; \quad (1)$$

and s_m is one of the APM symbols determined by the remaining $\log_2(M)$ information bits.

Example 2: Let us again consider the OSM scheme (Fig. 2), where $\mathbf{A} = \text{diag}\{1 \ 0 \ 0 \ 1\}$ as the first and fourth antennas are the selected antennas for Group 1 and Group 2, respectively. Given input bits “01”, $\Upsilon_1 = [1 \ 1 \ 0 \ 0]^T$ as Group 1 is chosen; and $s_1 = +1$. Thus, the transmitted signal is $\mathbf{x}_{1,1} = \mathbf{A}\Upsilon_1 s_1 = [+1 \ 0 \ 0 \ 0]^T$.

The received signal at the receiver of OSM-MISO, denoted as y , can then be given as

$$\begin{aligned} y &= \sqrt{p}\mathbf{h}\mathbf{x}_{k,m} + n = \sqrt{p}\mathbf{h}\mathbf{A}\Upsilon_k s_m + n \\ &\stackrel{(a)}{=} \sqrt{p} \sum_{j=(k-1)N_g+1}^{kN_g} a_j h_j s_m + n \stackrel{(b)}{=} \sqrt{p}g_{(k)}s_m + n \\ &\stackrel{(c)}{=} \sqrt{p}\mathbf{g}\mathbf{e}_k s_m + n \end{aligned} \quad (2)$$

where p is transmit power and n is the additive white Gaussian noise (AWGN) with zero-mean and σ^2 -variance; (a) follows for Group k transmission; (b) follows as Group k has only one active antenna $N_{(k)}$ with corresponding channel $g_{(k)}$; and (c) follows as $\mathbf{g} \in \mathbb{C}^{1 \times K} = [g_{(1)}, \dots, g_{(K)}]$ and $\mathbf{e}_k = [0, \dots, 1, \dots, 0]^T$ has “1” in the k th position and “0” else. Thus, OSM-MISO can be regarded as conventional SM-MISO with effective channel vector \mathbf{g} .

In conventional SM-MISO, the receiver uses the maximum likelihood (ML) detection criterion to jointly decode both the active antenna group index and the transmitted symbol. The same can be utilized for OSM-MISO. The ML decision rule is then given as

$$(\hat{k}, \hat{m}) = \arg \min_{k \in [1, K], m \in [1, M]} |y - \sqrt{p}g_{(k)}s_m|^2. \quad (3)$$

A critical quality measure of the ML detector is the symbol error probability (SEP), i.e., the probability that the detector chooses a symbol other than the actual transmit symbol. In order to analyze this measure, we define the set of all possible OSM transmit signals as $\mathbb{X} = \{\mathbf{x}_{k,m} = \mathbf{A}\Upsilon_k s_m \mid k = 1, \dots, K; m = 1, \dots, M\}$, with the size $|\mathbb{X}| = KM$. The elements of \mathbb{X} are equally likely.

Example 3: Let us again consider OSM-MISO in Fig. 2. The transmit signals set is given as $\mathbb{X} = \{[+1 \ 0 \ 0 \ 0]^T, [-1 \ 0 \ 0 \ 0]^T, [0 \ 0 \ 0 \ +1]^T, [0 \ 0 \ 0 \ -1]^T\}$.

Since each signal vector has only one non-zero element, the Hamming distance between any two $\mathbf{x}_{k,m}, \mathbf{x}_{k',m'} \in \mathbb{X}$ is either one or two. These two situations correspond to both signal vectors having same active antenna group index (i.e., $k = k'$) or not (i.e., $k \neq k'$). Based on these two situations, the average SEP, denoted as P_S , can be formulated as the sum of two terms (instead of three terms as in [29]):

$$P_S = \frac{1}{K} \sum_k P_{s_{\text{signal}}}(k) + \frac{1}{KM} \sum_k \sum_{k' \neq k} \sum_m \sum_{m'} \mathbb{E}_{\mathbf{h}} [\Pr\{\mathbf{x}_{k,m} = \mathbf{x}_{k',m'} \mid \mathbf{x}_{k,m}\}] \quad (4)$$

where

$$P_{s_{\text{signal}}}(k) = \frac{1}{M} \sum_m \sum_{m' \neq m} \mathbb{E}_{g_{(k)}} [\Pr\{s_m = s_{m'} \mid s_m\}]. \quad (5)$$

We can interpret this expression as follows:

- The first term $\frac{1}{K} \sum_k P_{s_{\text{signal}}}(k)$ is the SEP of OSM-MISO when $k = k'$. Only the modulated symbol is incorrectly detected, and $P_{s_{\text{signal}}}(k)$ can thus be regarded as the SEP of a conventional TAS-MISO for a given Group k antennas.
- The second term is the SEP of OSM-MISO when $k \neq k'$, so at least the antenna group index is incorrectly decoded.

The exact analysis of the P_S in (4) appears intractable due to the intricate second term. However, due to its low-complexity, Monte-Carlo simulation of OSM-MISO is easy to obtain in the low-to-moderate SNR region. But, in the high-SNR region, such simulations can be highly time-consuming. Therefore, analytical performance results for high-SNR are useful. For this reason, we focus on deriving an upper bound that is highly accurate for the high-SNR region. For this purpose, it is natural to consider the use of conventional union-bound, but the main challenge in (4) is the second term, and thus we will apply the union-bound to the second term only. This is known as the ‘‘Improved Union-bound’’ [29], a tighter upper bound of the SEP. This bound P_{IU} can be formulated as

$$P_S \leq P_{IU} = \frac{1}{K} \sum_k P_{s_{\text{signal}}}(k) + \frac{1}{KM} \sum_k \sum_{k' \neq k} \sum_m \sum_{m'} \text{APEP}_{(k,m) \rightarrow (k',m')} \quad (6)$$

where $\text{APEP}_{(k,m) \rightarrow (k',m')}$ is the average pairwise error probability (APEP) of $\mathbf{x}_{k,m}$ being erroneously decoded as

$\mathbf{x}_{k',m'} \in \mathbb{X}$, given as

$$\begin{aligned} \text{APEP}_{(k,m) \rightarrow (k',m')} &\triangleq \mathbb{E}_{\mathbf{h}} [\Pr(\mathbf{x}_{k,m} \rightarrow \mathbf{x}_{k',m'} \mid \mathbf{h})] \\ &= \mathbb{E}_{\mathbf{h}} [\Pr(|y - \sqrt{p}\mathbf{h}\mathbf{x}_{k,m}|^2 \geq |y - \sqrt{p}\mathbf{h}\mathbf{x}_{k',m'}|^2 \mid \mathbf{h})] \\ &= \mathbb{E}_{\mathbf{g}} [\Pr(|y - \sqrt{p}g_{(k)}s_m|^2 \geq |y - \sqrt{p}g_{(k')}s_{m'}|^2 \mid \mathbf{g})] \\ &= \mathbb{E}_{\mathbf{g}} \left[Q \left(\sqrt{\frac{p|g_{(k)}s_m - g_{(k')}s_{m'}|^2}{2\sigma^2}} \right) \right] \triangleq \mathbb{E}_{\mathbf{g}} \left[Q \left(\sqrt{\frac{\gamma\Psi^2}{2}} \right) \right] \end{aligned} \quad (7)$$

with $Q(\cdot)$ being the Gaussian Q-function, $\gamma \triangleq \frac{p}{\sigma^2}$ being the Signal-to-Noise Ratio (SNR), and $\Psi \triangleq |g_{(k)}s_m - g_{(k')}s_{m'}|, k \neq k'$. Note that $\sqrt{p}\Psi$ indicates the Euclidean distance (ED) between two possible received signals $\sqrt{p}g_{(k)}s_m$ and $\sqrt{p}g_{(k')}s_{m'}$ from different transmit antennas ($k \neq k'$) in the receive OSM constellation.

Remark 2: Special cases: i) When $K = 1$, we have $N_g = N_t$ and $\mathbf{g} = g_{(1)}$ which is conventional TAS-MISO. Then, the second term of (6) vanishes, and $P_S = P_{IU} = P_{s_{\text{signal}}}(1)$; ii) if $M = 1$, i.e., opportunistic space shift keying (OSSK)-MISO case, the first term of (6) vanishes, and (6) reduces as $P_S \leq P_{IU} = \frac{1}{K} \sum_k \sum_{k' \neq k} \text{APEP}_{k \rightarrow k'}$ with $\text{APEP}_{k \rightarrow k'} = \mathbb{E}_{\mathbf{g}} \left[Q \left(\sqrt{\frac{\gamma|g_{(k)} - g_{(k')}|^2}{2}} \right) \right], k \neq k'$. Although OSSK-MISO is beyond the scope of this paper, the OSM-MISO ($M \geq 2$) results can be easily extended to the OSSK-MISO ($M = 1$).

III. PERFORMANCE ANALYSIS OF OSM-MISO

Here we derive the closed-form expression of improved upper-bound of SEP given in (6) with M-PSK and the explicit asymptotic SEP behavior in the high SNR region. The extension to the QAM modulation case is also discussed.

A. Explicit Error Performance of OSM-MISO

We first derive the exact $\frac{1}{K} \sum_k P_{s_{\text{signal}}}(k)$, i.e., the first term of (6). As mentioned before, $P_{s_{\text{signal}}}(k)$ is the exact SEP of conventional TAS-MISO with the selected best channel $g_{(k)}$. According to [30, eq.(30)] [31, eq. (5.66)], $P_{s_{\text{signal}}}(k)$ only depends on the distribution of its channel gain $|g_{(k)}|^2$. Given iid Rayleigh channel, according to [32], the pdf of the selected best channel gain for k -th antenna group ($z_k = |g_{(k)}|^2 = \max_{i \in [(k-1)N_g+1, kN_g]} |h_i|^2$) is given as

$$f(z_k) = N_g (1 - e^{-z_k})^{N_g-1} e^{-z_k}, \quad k = 1, \dots, K. \quad (8)$$

As all $|g_{(1)}|^2, \dots, |g_{(K)}|^2$ are also iid, we can obtain $P_{s_{\text{signal}}}(1) = \dots = P_{s_{\text{signal}}}(K) \triangleq P_{s_{\text{signal}}}$, i.e., $\frac{1}{K} \sum_k P_{s_{\text{signal}}}(k) = P_{s_{\text{signal}}}$. Then based on [30] and [31] and the distribution (8), the closed-form expression for $P_{s_{\text{signal}}}$ for M -PSK signaling is given in Proposition 1.¹

¹One may obtain the closed-form of $P_{s_{\text{signal}}}$ directly from [30, eq. (33)], but it involves N_g infinite sums, which is too complicated. Here, we provide a simpler expression based on the Binomial theorem and [31, eq. (5A.15)].

Proposition 1: With M -PSK modulation, the exact expression of $P_{s_{\text{signal}}} = P_{s_{\text{signal}}}(k), \forall k$ is

$$P_{s_{\text{signal}}} = \frac{M-1}{M} - \sum_{n=0}^{N_g-1} \binom{N_g}{n+1} \frac{(-1)^n}{\pi} \sqrt{\frac{\sin^2\left(\frac{\pi}{M}\right)}{\frac{1}{\bar{\gamma}}(1+n) + \sin^2\left(\frac{\pi}{M}\right)}} \times \left[\frac{\pi}{2} + \tan^{-1} \left(\sqrt{\frac{\sin^2\left(\frac{\pi}{M}\right)}{\frac{1}{\bar{\gamma}}(1+n) + \sin^2\left(\frac{\pi}{M}\right)}} \cot\left(\frac{\pi}{M}\right) \right) \right]. \quad (9)$$

Proof: See Appendix A. ■

Now, we derive the closed-form for the second term of (6). From (7), in order to obtain the analytic expression of $\text{APEP}_{(k,m) \rightarrow (k',m')}$, we must know the distribution of Ψ . This is a challenging task, but we tackle this impediment. The complex random variable $g_{(k)}$ can be written as $g_{(k)} = r_k e^{j\theta_k}$, $k = 1, \dots, K$, where $r_k = |g_{(k)}|$ and θ_k is the phase of $g_{(k)}$. For M -PSK, the symbols can be given as $s_m = e^{j\frac{2\pi m}{M}}, \forall m = 1, \dots, M$. We thus have

$$\begin{aligned} \Psi &= \left| r_k e^{j(\theta_k + \frac{2\pi m}{M})} - r_{k'} e^{j(\theta_{k'} + \frac{2\pi m'}{M})} \right| \\ &= \left| r_k e^{j(\theta_k + \frac{2\pi m}{M})} + r_{k'} e^{j(\theta_{k'} + \frac{2\pi m'}{M} + \pi)} \right| \end{aligned} \quad (10)$$

The PDFs of r_k and θ_k are given in the following Lemma 1.

Lemma 1: Given that $g_{(k)} = r_k e^{j\theta_k}$, $k = 1, \dots, K$, $r_k = |g_{(k)}|, \forall k$ are iid. with PDF given as

$$f_{r_k}(x) = 2N_g x e^{-x^2} \left(1 - e^{-x^2}\right)^{N_g-1}. \quad (11)$$

The phase θ_k is uniformly distributed over the range $[0, 2\pi]$, i.e., $f_{\theta_k}(y) = \frac{1}{2\pi}$. And r_k and θ_k are independent.

Proof: See Appendix B. ■

Lemma 1 shows that r_k and $r_{k'}$ are iid., so are θ_k and $\theta_{k'}$; $\theta_k + \frac{2\pi m}{M}$ and $\theta_{k'} + \frac{2\pi m'}{M} + \pi$ are also uniformly distributed in $[0, 2\pi]$. This also implies that the M -PSK symbols have no impact on Ψ . By using the result of the distribution for the magnitude of the sum of complex random variables [33, eq. (10)], the PDF of Ψ can be given as

$$f_{\Psi}(x) = x H_{0x} \{ \Lambda(\rho) \} \quad (12)$$

where $H_{0x} \{ \Lambda(\rho) \} = \int_0^\infty \rho J_0(x\rho) \Lambda(\rho) d\rho$ is the zero-order Hankel transform of function $\Lambda(\rho)$, $J_0(\cdot)$ is the zero-order Bessel function of the first kind, and

$$\Lambda(\rho) = \mathbb{E}_{r_k, r_{k'}} [J_0(r_k \rho) J_0(r_{k'} \rho)]. \quad (13)$$

Based on Lemma 1 and (12), we derive Lemma 2 and Proposition 2.

Lemma 2: The PDF of Ψ in (10) can be derived as

$$f_{\Psi}(x) = \sum_{n=0}^{N_g-1} \sum_{l=0}^{N_g-1} \frac{2(N_g!)^2 (-1)^{n+l} x e^{-\frac{(n+l+1)x^2}{n+l+2}}}{n!(N_g-1-n)!l!(N_g-1-l)!(n+l+2)} \quad (14)$$

Proof: See Appendix C. ■

Proposition 2: The closed-form $\text{APEP}_{(k,m) \rightarrow (k',m')}$ can be derived as

$$\begin{aligned} \text{APEP}_{(k,m) \rightarrow (k',m')} &= \sum_{n=0}^{N_g-1} \sum_{l=0}^{N_g-1} \binom{N_g}{n+1} \binom{N_g}{l+1} \frac{(-1)^{n+l}}{2} \\ &\times \left[1 - \left(1 + \frac{4(n+l+1)}{\bar{\gamma}(n+l+2)} \right)^{-\frac{1}{2}} \right]. \end{aligned} \quad (15)$$

Proof: For $a > 0$ and $b > 0$, we have $\int_0^\infty Q(ax) x e^{-bx^2} dx = \frac{1}{4b} \left[1 - (1 + 2b/a^2)^{-\frac{1}{2}} \right]$. Thus, performing the average in (7) by applying (14), we get (15). ■

Remark 3: Interestingly, Proposition 2 shows that given $k \neq k'$ and M -PSK, the expression $\text{APEP}_{(k,m) \rightarrow (k',m')}$ in (15) does not depend on any symbol or antenna information, which implies $\text{APEP}_{(k,m) \rightarrow (k',m')}$ is identical for any given set of $\{k, k', m, m'\}$. This is because i) all selected channels are iid; and ii) as shown in (10), the effective phase distributions of channels after absorbing the impact of symbols are still iid uniformly distributed.

Based on Proposition 2 and Remark 3, for presentation simplicity, we denote $\overline{\text{APEP}} = \text{APEP}_{(k,m) \rightarrow (k',m')}, \forall k \neq k', \forall m, m'$. Therefore, an explicit improved union-bound of the OSM-MISO scheme can be stated as

$$\begin{aligned} P_{IU} &= P_{s_{\text{signal}}} + M(K-1) \overline{\text{APEP}} \\ &= \frac{M-1}{M} - \sum_{n=0}^{N_g-1} \binom{N_g}{n+1} \frac{(-1)^n}{\pi} \sqrt{\frac{\sin^2\left(\frac{\pi}{M}\right)}{\frac{1}{\bar{\gamma}}(1+n) + \sin^2\left(\frac{\pi}{M}\right)}} \\ &\times \left[\frac{\pi}{2} + \tan^{-1} \left(\sqrt{\frac{\sin^2\left(\frac{\pi}{M}\right)}{\frac{1}{\bar{\gamma}}(1+n) + \sin^2\left(\frac{\pi}{M}\right)}} \cot\left(\frac{\pi}{M}\right) \right) \right] \\ &+ M(K-1) \sum_{n=0}^{N_g-1} \sum_{l=0}^{N_g-1} \binom{N_g}{n+1} \binom{N_g}{l+1} \frac{(-1)^{n+l}}{2} \\ &\times \left[1 - \left(1 + \frac{4(n+l+1)}{\bar{\gamma}(n+l+2)} \right)^{-\frac{1}{2}} \right]. \end{aligned} \quad (16)$$

Remark 4 (Best (K, M) Pair): for a given number of transmit antennas N_t , to convey a target information bits B , (16) suggests there is an optimal pair (K, M) , among various configurations of signal and spatial constellations of OSM-MISO, that minimizes the ABEP performance, given as,

$$\begin{aligned} \min_{K, M} P_S &\leq P_{IU} \\ \text{s.t. } \log_2(K) + \log_2(M) &= B. \end{aligned} \quad (17)$$

This optimal information bit allocation is also known as the optimal interplay of signal and spatial constellation diagrams [29]. Here we call it best ‘bi-constellation selection’ (BCS).

B. Explicit Asymptotic Error Performance of OSM-MISO

We now study the asymptotic error performance of OSM-MISO scheme in the high SNR region, i.e., $\bar{\gamma} \rightarrow \infty$.

Based on Proposition 1, we first give an asymptotic $P_{s\text{signal}}$ in Proposition 3.

Proposition 3: In the high SNR region ($\bar{\gamma} \rightarrow \infty$), $P_{s\text{signal}}$ can be written as

$$P_{s\text{signal}} = \frac{\frac{\Gamma(N_g + \frac{1}{2})}{2\sqrt{\pi}} + \frac{N_g!}{\pi} \cos\left(\frac{\pi}{M}\right) {}_2F_1\left(\frac{1}{2}, \frac{1}{2} - N_g; \frac{3}{2}; \cos^2\left(\frac{\pi}{M}\right)\right)}{\sin^{2N_g}\left(\frac{\pi}{M}\right) \bar{\gamma}^{N_g}} + \mathcal{O}\left(\frac{1}{\bar{\gamma}^{N_g+1}}\right) \quad (18)$$

where ${}_2F_1(\cdot, \cdot; \cdot; \cdot)$ is the Gauss hypergeometric function.

Proof: See Appendix D ■

This result is consistent with [30, eq. (35)] for TAS-MISO over Rayleigh fading. We next derive an asymptotic expression for $\overline{\text{APEP}}$ in Proposition 4.

Proposition 4: In the high SNR region ($\bar{\gamma} \rightarrow \infty$), $\overline{\text{APEP}}$ can be recast as

$$\overline{\text{APEP}} = \frac{N_g}{4N_g - 2} \frac{1}{\bar{\gamma}} + \mathcal{O}\left(\frac{1}{\bar{\gamma}^2}\right). \quad (19)$$

Proof: See Appendix E ■

Remark 5: Proposition 4 implies the diversity order of term $\overline{\text{APEP}}$ is one. This is because, according to (7) and (10), the phase difference between any two possible received signals from different transmit antennas, i.e., $\sqrt{p}g_{(k)sm}$ and $\sqrt{p}g_{(k')sm'}$ with $k \neq k'$, in the receive constellation diagram is $\theta_k - \theta_{k'} + \frac{2\pi(m'-m)}{M}$, which is a random variable and may lead to the case of different antennas yielding similar received signals. As a result, the information conveyed by the antenna positions may not be uniquely decodable.

By substituting Proposition 3 and Proposition 4 into (16), we can obtain the error rate of our proposed OSM-MISO at high SNR as follows.

- 1) When $K = 1$, i.e., conventional TAS-MISO case, we have $N_g = N_t$ and

$$P_s = P_{IU} = P_{s\text{signal}}|_{N_g=N_t} = \frac{N_t!}{\sin^{2N_t}\left(\frac{\pi}{M}\right)} \left[\frac{\Gamma(N_t + \frac{1}{2})}{2\sqrt{\pi}N_t!} + \frac{\cos\left(\frac{\pi}{M}\right)}{\pi} {}_2F_1\left(\frac{1}{2}, \frac{1}{2} - N_t; \frac{3}{2}; \cos^2\left(\frac{\pi}{M}\right)\right) \right] \frac{1}{\bar{\gamma}^{N_t}} + \mathcal{O}\left(\frac{1}{\bar{\gamma}^{N_t+1}}\right) \quad (20)$$

The error performance is determined by $P_{s\text{signal}}$ only, and the full transmit diversity order N_t can be achieved.

- 2) When $K = N_t$, i.e., conventional SM case, we have $N_g = 1$ and

$$P_{IU} = P_{s\text{signal}}|_{N_g=1} + M(K-1)\overline{\text{APEP}}|_{N_g=1} = \left[\frac{1}{4\sin^2\left(\frac{\pi}{M}\right)} + \frac{\cos\left(\frac{\pi}{M}\right) {}_2F_1\left(\frac{1}{2}, -\frac{1}{2}; \frac{3}{2}; \cos^2\left(\frac{\pi}{M}\right)\right)}{\pi \sin^2\left(\frac{\pi}{M}\right)} \right] \frac{1}{\bar{\gamma}} + \frac{(N_t-1)M}{2} \left[\frac{1}{\bar{\gamma}} + \mathcal{O}\left(\frac{1}{\bar{\gamma}^2}\right) \right]. \quad (21)$$

This is consistent with the well-known result of the conventional SM scheme [29], for which the diversity order is just one.

- 3) When $1 < K < N_t$, i.e., $1 < N_g < N_t$, by considering the effective term at high SNR based on $P_{IU} = P_{s\text{signal}} + M(K-1)\overline{\text{APEP}}$ in (16), we have

$$P_{IU} = \frac{M(K-1)N_t}{4N_t - 2K} \frac{1}{\bar{\gamma}} + \mathcal{O}\left(\frac{1}{\bar{\gamma}^2}\right). \quad (22)$$

As the above two extreme cases $K = 1$ and $K = N_t$ achieve transmit diversity order N_t and 1, respectively, one may expect that $1 < K < N_t$ case can achieve diversity order somewhere in between one and N_t . But (22) shows an interesting result that in this case, the diversity order is still one, as the OSM-MISO error performance is dominated by $\overline{\text{APEP}}$.

Remark 6 (Coding Gain Difference): According to [34], the coding gain of (21) and (22) can be defined respectively as

$$C_{SM} \triangleq \left[\frac{1}{4\sin^2\left(\frac{\pi}{M}\right)} + \frac{\cos\left(\frac{\pi}{M}\right) {}_2F_1\left(\frac{1}{2}, -\frac{1}{2}; \frac{3}{2}; \cos^2\left(\frac{\pi}{M}\right)\right)}{\pi \sin^2\left(\frac{\pi}{M}\right)} + \frac{(N_t-1)M}{2} \right]^{-1}$$

and $C_{1 < K < N_t} \triangleq \frac{4N_t - 2K}{M(K-1)N_t} = \frac{4N_t - 2K}{2^B(1 - \frac{1}{K})^{N_t}}$. With given N_t and fixed data rate $B = \log(KM)$, it is easy to show that the coding gain $C_{1 < K < N_t}$ is monotonically increasing as K decreases. Then, we have $C_{1 < K < N_t} > \frac{4N_t - 2K}{M(K-1)N_t}|_{K=N_t} = \frac{2}{(N_t-1)M}$. Due to $C_{SM} < \left[\frac{(N_t-1)M}{2} \right]^{-1}$, we also have $C_{SM} < C_{1 < K < N_t}$. This is an important finding as it implies that although both two cases (21) and (22) have the same diversity, the SEP of OSM-MISO with $1 < K < N_t$ provides higher coding gain than that of the conventional SM, and this benefit becomes more pronounced as K decreases.

Remark 7 (BCS in the High SNR Region & Overall Coding Gain Trend): By comparing (20), (21) and (22), we find that in the high SNR region, for optimization problem (17) with given N_t and fixed SE (i.e., data rate B is fixed), the average error performance can be minimized by using the smallest number of antenna groups ($K = 1$) and the highest possible constellation size ($M = 2^B$), as this combination achieves the full-diversity order N_t . In other words, the constellations configuration of $(1, 2^B)$ is always the BCS for high SNRs. Thus, together with Remark 6, we can conclude that with given N_t and fixed SE, the coding gain trend of OSM-MISO for any $1 \leq K \leq N_t$, is monotonically increasing as K decreases. This is a very interesting trend as it implies that at high SNR, the error performance of OSM-MISO is substantially improved by using fewer antenna groups K and larger signal constellation size M . Based on this trend, we also can obtain the SNR crossing point $\bar{\gamma}_0$ for always using BCS $(1, 2^B)$ pair in high SNR region $[\bar{\gamma}_0, \infty)$, i.e., the $\bar{\gamma}_0 = \bar{\gamma}$ with $\bar{\gamma}$ satisfied $P_{IU}|_{K=1} \geq P_{IU}|_{K=2}$ in (17).

C. OSM and Other TASS-SM Schemes

We compare our proposed OSM with two existing TASS-SM schemes [14]: i) Capacity Optimized Antenna

Selection aided SM (COAS-SM); and ii) Euclidean Distance optimized Antenna Selection aided SM (EDAS-SM).

1) *OSM and COAS-SM Comparison*: COAS-SM is also a low-complex TASS-SM scheme, where K out of N_t transmit antennas (with the K largest channel gains) are chosen for operating SM with M -ary APM symbols. Despite different antenna selections, OSM and COAS-SM both offer the same data throughput $B = \log_2(KM)$ bpcu, and have identical set-up when $K = 1$ (pure TAS) and $K = N_t$ (conventional SM). However when $1 < K < N_t$, the two schemes have significantly dissimilar set-ups, and our OSM offers the following advantages over COAS-SM.

- **Analytical tractability**: Due to the unique feature of independent group antenna selection, analytical bounds and asymptotic expressions of OSM are tractable (Section III). In contrast, such analysis is challenging for COAS-SM [14]. The reason is that ordered channel amplitudes associated with the selected K antennas are not independent. It is thus difficult to derive a tractable distribution of $|g_{(k)}s_m - g_{(k')}s_{m'}|, k \neq k'$ for COAS-SM, which is the key for the APEP analysis (7). The problem is greatly exacerbated for large K .
- **Reduced CSI feedback overhead**: Both schemes require the receiver to send the selected antenna indexes to the transmitter. While OSM requires $K \log_2 \frac{N_t}{K}$ feedback bits, COAS-SM requires $\log_2 \binom{N_t}{K}$ feedback bits which is much larger, especially for large N_t , e.g., when $N_t = 32$ and $K = 8$, OSM and COAS-SM schemes require at least 16 and 24 bits feedback, respectively.
- **Low complexity**: OSM-MISO offers complexity saving in two ways:
 - 1) **Antenna selection** - while OSM requires sorting $\frac{N_t}{K}$ elements K times, COAS-SM needs sorting N_t elements which costs higher computations, e.g., when $N_t = 32$ and $K = 16$, the computational complexity (for majority serial sorting algorithms, such as Quicksort and Heapsort, the average complexity is $\mathcal{O}(n \log n)$) of the COAS-SM scheme is about five times higher than that of the OSM scheme.
 - 2) **Simulation time** - Since COAS-SM lacks rigorous analytical error rate expressions, Monte-Carlo simulations are required. Especially at high-SNR, COAS-SM consumes significant time for simulations (to estimate an error rate of 10^{-4} , 10^7 channel realizations may be needed). And the problem is dramatically aggravated for large N_t and/or B . Conversely, the OSM high-SNR performance can be easily computed by the derived explicit expressions.
- **Superior high-SNR performance**: Both offer similar performance at low SNR for $N_t \geq 8$, but OSM provides higher coding gain as SNR increases. Their performances are compared in detail in Section IV.

2) *OSM and EDAS-SM Comparison*: EDAS-SM selects K antennas out of N_t that maximizes the minimum ED of the received SM constellation (a dominant factor of the error performance). It needs to search exhaustively over all $\binom{N_t}{K}$ antenna subsets. Consequently, EDAS-SM provides excellent error performance, albeit at the cost of high computational

complexity and intractable analysis. Compared to EDAS-SM, OSM-MISO still attains most of the above listed benefits, i.e., analytical tractability, reduced CSI feedback bits, and low computational complexity. According to [18], the exhaustive search of EDAS-SM-MISO [14] requires in total $4 \binom{N_t}{2} M^2$ flops (floating point operations), which is significantly higher than the OSM especially for large signal constellation size, and limits its practicality. Thus, although EDAS-SM outperforms OSM (Section IV), the latter offers an attractive performance-complexity trade-off.

D. Extension to QAM:

The analysis up to this point assumes M -ary PSK modulation, for which we derived a closed-form expression for improved union-bound P_{IU} in Eq. (16) and the high SNR analysis (20)-(22). We now extend this analysis to OSM-MISO with QAM modulation.

More specifically, when the square M-QAM constellation (with $M = 2^{2n}, \forall n \in \mathbb{N}$) is considered, the symbols set can be expressed as $\mathbb{S}_{QAM} = \frac{1}{\sqrt{\frac{M}{2}(M-1)}} \{a + bj, a - bj, -a + bj, -a - bj\}$, where $a, b \in \{1, 3, \dots, M-1\}$ [23]. With M-QAM modulation, similar to Proposition 1, the exact expression of P_{signal} can be obtained from [30, eq. (39)]. From (7), with M-QAM, we have $\text{APEP}_{(k,m) \rightarrow (k',m')} \triangleq \mathbb{E}_g \left[Q \left(\sqrt{\frac{\tilde{\gamma} \Psi^2}{2}} \right) \right]$ with $\Psi = |g_{(k)}s_m - g_{(k')}s_{m'}|, k \neq k'$, where $s_m, s_{m'} \in \mathbb{S}_{QAM}$. The complex M-QAM symbols can be written as $s_m = |s_m|e^{j\omega_m}, m = 1, \dots, M$, where ω_m is the phase of symbol s_m . Then we have $\Psi = \left| |s_m|r_k e^{j(\theta_k + \omega_m)} + |s_{m'}|r_{k'} e^{j(\theta_{k'} + \omega_{m'} + \pi)} \right|$. Thus, following the similar analysis of (12)-(15), we can get the closed-form expression of $\text{APEP}_{(k,m) \rightarrow (k',m')}$ with M-QAM, i.e.,

$$\begin{aligned} \text{APEP}_{(k,m) \rightarrow (k',m')} &= \sum_{n=0}^{N_g-1} \sum_{l=0}^{N_g-1} \binom{N_g}{n+1} \binom{N_g}{l+1} \frac{(-1)^{n+l}}{2} \\ &\times \left[1 - \left(1 + \frac{4(n+1)(l+1)}{\tilde{\gamma}(|s_{m'}|^2(n+1) + |s_m|^2(l+1))} \right)^{-\frac{1}{2}} \right], \end{aligned}$$

which, unlike the M-PSK case as stated in Remark 3, does depend on symbols information. Applying the obtained explicit expressions of P_{signal} and $\text{APEP}_{(k,m) \rightarrow (k',m')}$ into (6), i.e., $P_{IU} = P_{\text{signal}} + \frac{1}{KM} \sum_k \sum_{k' \neq k} \sum_m \sum_{m'} \text{APEP}_{(k,m) \rightarrow (k',m')}$, we also get the closed-form expression of improved union-bound P_{IU} for OSM-MISO with M-QAM.

The high SNR analysis (Section III-B) can be easily extended to the QAM case too. According to [30, eq. (40)], as $\tilde{\gamma} \rightarrow \infty$, P_{signal} for OSM-MISO with QAM can be given as

$$\begin{aligned} P_{\text{signal}} &= \frac{1}{\left(\frac{3}{M-1}\right)^{N_g} \tilde{\gamma}^{N_g}} \left[\frac{2^{N_g+1} \left(1 - \frac{1}{\sqrt{M}}\right) \Gamma(N_g + \frac{1}{2})}{\sqrt{\pi}} \right. \\ &\quad \left. - \frac{N_g! \left(1 - \frac{1}{\sqrt{M}}\right)^2}{\pi (N_g + \frac{1}{2})} F_1 \left(1, N_g, 1; N_g + \frac{3}{2}; \frac{1}{2}, \frac{1}{2} \right) \right] \\ &\quad + \mathcal{O} \left(\frac{1}{\tilde{\gamma}^{N_g+1}} \right) \end{aligned} \quad (23)$$

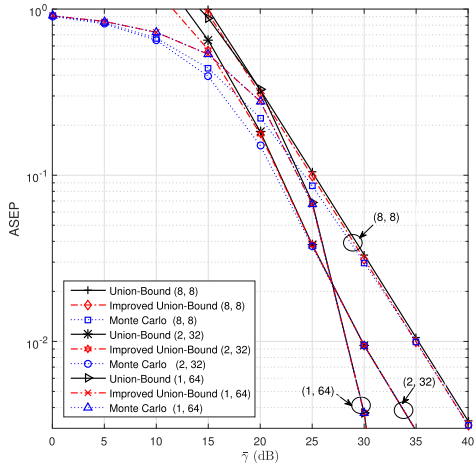


Fig. 3. Conventional union-bound, improved union-bound and Monte Carlo simulations when $N_t = 8$ and $B = 6$ bits.

where $F_1(\cdot, \cdot, \cdot; \cdot; \cdot, \cdot)$ is the Appell hypergeometric function [30]. Following similar analysis on that in Proposition 4, the asymptotic expression of $\text{APEP}_{(k,m) \rightarrow (k',m')}$ for OSM-MISO with QAM at high SNR, can be written as,

$$\begin{aligned} \text{APEP}_{(k,m) \rightarrow (k',m')} &= \sum_{n=0}^{N_g-1} \sum_{l=0}^{N_g-1} \binom{N_g}{n+1} \binom{N_g}{l+1} \\ &\quad \times \frac{(-1)^{n+l} (n+1)(l+1)}{(|s'_m|^2(n+1) + |s_m|^2(l+1))\bar{\gamma}} \\ &\quad + \mathcal{O}\left(\frac{1}{\bar{\gamma}^2}\right). \end{aligned} \quad (24)$$

By substituting (23) and (24) into (6), similar high SNR analysis discussion as (20)-(22) can be obtained and like the PSK case, OSM-MISO with QAM achieves full-diversity order for $(K, M) = (1, 2^B \text{QAM})$, but only offers diversity order one for all other pairs. The details are omitted to avoid repetition. The simulation can be found in Section IV-D.

IV. NUMERICAL RESULTS

In this section, we validate the analytical results (Section III), and evaluate the performance of our OSM-MISO via numerical simulations and comparisons made with other TASS-SM-MISO schemes such as COAS-SM-MISO and EDAS-SM-MISO. It is important to note that, for a given N_t with fixed data rate B , there exists a few different combinations of the sizes of spatial constellation (i.e., K) and signal constellation (i.e., M), which satisfy the targeted SE of $\log_2(KM) = B$. The combination pair of K and M is denoted as (K, M) .

A. Performance of OSM-MISO

Fig. 3 plots the SEP with the average SNR for OSM-MISO when $N_t = 8$ and $B = 6$ bits. We consider three possible combinations: $(K, M) = \{(1, 64), (2, 32), (8, 8)\}$ (note that to avoid clutter, $(K, M) = (4, 16)$ is not plotted). Fig. 3 also examines the accuracy of the improved union-bound (analytical expression (16)), by comparing it with Monte Carlo

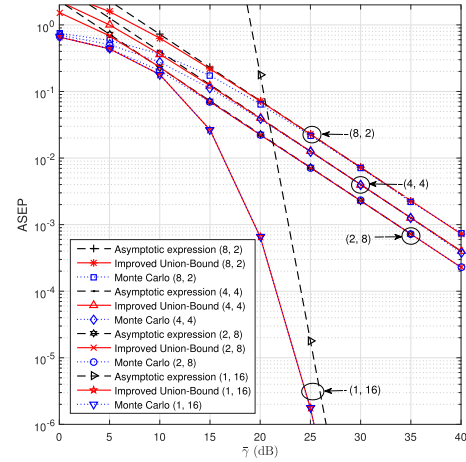


Fig. 4. SEP via asymptotic expression, improved union-bound and Monte Carlo simulations when $N_t = 8$ and $B = 4$ bits.

simulations and the conventional union-bound (calculated by applying union-bound to both terms of (4)). Note that the improved union-bound is always closer to simulation results than the conventional union-bound. In particular, unlike the latter, the improved union-bound is almost identical with Monte Carlo results over the entire SNR region when $K = 1$ (i.e., conventional TAS-MISO case), which agrees with Remark 2 of Section II. For any $K \geq 2$ cases, the improved union-bound better overlaps with Monte Carlo simulations over moderate or high SNR region. This validates the accuracy and tightness of the derived improved union-bound of OSM-MISO in (16). More importantly, it can be calculated efficiently for any B and N_t as it does not include special functions. This is a key advantage over intensive Monte Carlo.

Fig. 4 depicts the SEP with the average SNR of OSM-MISO when $N_t = 8$ and $B = 4$ bits, for $(K, M) = \{(8, 2), (4, 4), (2, 8), (1, 16)\}$. This figure evaluates OSM-MISO asymptotic results from (20), (21) or (22). Just like the accuracy of improved union-bound in Fig. 3, the asymptotic results match well the Monte Carlo simulations at high SNR, which confirms the asymptotic-exactness of our analysis in Section III-B. The OSM-MISO achieves full-diversity order for $(K, M) = (1, 16)$, but only offers diversity order one for $(K, M) = (8, 2)$ (conventional SM case), $(K, M) = (4, 4)$ and $(K, M) = (2, 8)$ case. This implies that, for a given N_t and fixed B , the case $(K, M) = (1, 2^B)$ achieves the best performance among all possible combinations of (K, M) at high SNR due to the diversity advantage, which confirms Remark 7 in the Section III-B. Although having the same diversity order, as shown in Fig. 4, with given N_t and fixed B , OSM-MISO with any $1 < K < N_t$ (i.e., $(K, M) = (4, 4)$ or $(K, M) = (2, 8)$) has significantly higher coding gain than that of conventional SM, and the coding gain of OSM-MISO increases monotonically as K decreases, which agrees with Remark 6 in Section III-B. For example, the Table I lists the coding gain comparison between conventional SM and OSM-MISO with $1 < K < N_t$, which shows the coding gain order is $(K, M) = (8, 2) < (K, M) = (4, 4) < (K, M) = (2, 8)$.

TABLE I
THE CODING GAIN DIFFERENCE BETWEEN CONVENTIONAL
SM AND THE OSM-MISO WITH $1 < K < N_t$

Comparison	$N_t = 8$ and $B = 4$		
(K, M)	(8,2)	(4,4)	(2,8)
coding gain	-8.6 dB	-6.0 dB	-3.6 dB

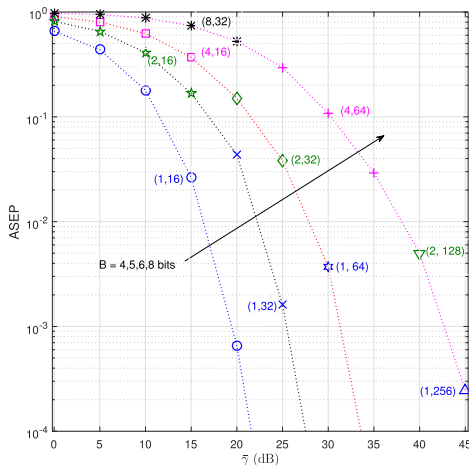


Fig. 5. SEP of OSM-MISO with BCS for $N_t = 8$ and $B = 4, 5, 6, 8$ bits.

B. Interplay of K and M (BCS)

Fig. 3 and Fig. 4, for given N_t and B , suggest an optimal configuration among all the possible combinations of (K, M) , that gives the best SEP performance at a given SNR, i.e., the BCS, as we mentioned in Remark 4. For example, in Fig. 3 with $B = 6$ bits, $(2, 32)$ and $(1, 64)$ pairs achieve the minimum SEP at $\bar{\gamma} = 20$ dB and $\bar{\gamma} = 30$ dB, respectively. While, for $B = 4$ bits in Fig.4, $(1, 16)$ is always the winner at any SNR. However, in general, there is no clear-cut answer as to which (K, M) is optimal to minimize the SEP for a given set of N_t and B except for the high-SNR region (Remark 7).

To further explore the BCS characteristics, Fig. 5 plots the SEP of OSM-MISO with BCS at each SNR² for given $N_t = 8$ and $B = 4, 5, 6, 8$ bits, respectively. The SNR range is $\bar{\gamma} \in [0, 45]$ dB with 5 dB steps. Please note that we find the best (K, M) pair by exhaustive search. A discrete mark on the plot represents the best (K, M) combination for a particular set of B and $\bar{\gamma}$. For the sake of clarity, we connect the best (K, M) combinations for that particular B with a dotted line. As shown in Fig. 5, $(1, 16)$ is the best for small data rate $B = 4$ bits within the entire simulated SNR region. As we increase B (from 5 bits onwards), the number of dissimilar BCS among the SNR range is gradually rising until it reaches its maximum. For example, for $B = 5$ bits, $(2, 16)$ is the BCS for $\bar{\gamma} = [0, 15]$ dB while $(1, 32)$ is the best pair for $\bar{\gamma} \geq 20$ dB; when $B = 8$ bits, we sequentially have $(8, 32)$, $(4, 64)$, $(2, 128)$ and $(1, 256)$ in order to be the BCS pair as SNR increases in the range of $[0, 45]$ dB]. But for any cases, $(1, 2^B)$ is always the BCS for the high SNR regime due to its highest transmit

²Note that, from now on, the SEP of OSM-MISO is estimated via Monte Carlo simulations at low or moderate SNR and the improved union-bound as an accurate and efficient alternative at high SNR.

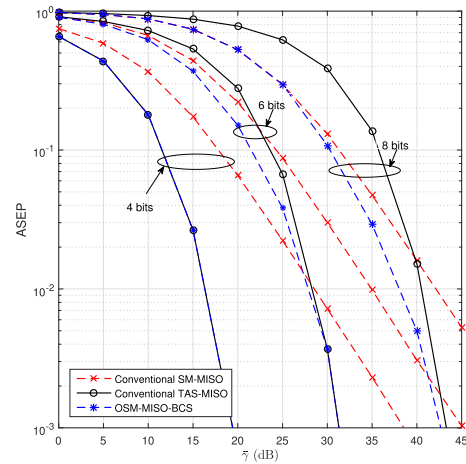


Fig. 6. SEP of conventional SM-MISO, conventional TAS-MISO and OSM-MISO with BCS for $N_t = 8$ and $B = 4, 6, 8$ bits.

diversity, which agrees with Remark 7. Therefore, for fixed N_t and data rate B , as SNR increases, fewer antenna groups K and larger signal modulation order M seem to achieve the optimal SEP performance.

Fig. 6 compares the SEP performance of BCS-based OSM-MISO (denoted as OSM-MISO-BCS), conventional TAS-MISO (OSM-MISO with $K = 1$) and conventional SM-MISO (OSM-MISO with $K = N_t$), for $N_t = 8$ with 4, 6, 8 bits data rate, respectively. As shown in Fig.6, for $B = 4$ bits, the OSM-MISO-BCS and conventional TAS-MISO have identical performance since $(1, 2^B)$ is always the best configuration pair for small B as we mentioned above. As the data throughput increases, while the SEP performance of OSM-MISO-BCS always approaches conventional TAS-MISO in the high SNR regime as expected, OSM-MISO-BCS significantly outperforms conventional TAS-MISO at low and moderate SNR, especially for large B . For instance, to achieve 10^{-1} SEP with $B = 6$ bits and $B = 8$ bits, OSM-MISO-BCS saves approximately 2.11 dB and 5.43 dB power over conventional TAS-MISO, respectively. On the other hand, for any given B , OSM-MISO-BCS offers significant performance gap over conventional SM-MISO especially at high SNR. For example, for a target SEP of 10^{-2} , OSM-MISO-BCS offers around 12.22 dB, 7.08 dB and 4.10 dB power reduction compared with conventional SM-MISO for $B = 4, 6, 8$ bits, respectively. However, for $B = 8$ bits, the SEP of OSM-MISO-BCS approaches that of conventional SM-MISO at low SNR.

C. Comparison of OSM-MISO, COAS-SM-MISO and EDAS-SM-MISO

Fig.7 compares the SEPs of OSM-MISO and COAS-SM-MISO, for $N_t = 16$ with $B = 4, 6, 8$ bits, respectively, where we consider $K = 2$ and $K = 8$ for each B . Note that given K and B , the value of M can be simply calculated by $M = \frac{2^B}{K}$. Although both schemes have similar SEP at low SNR, as SNR increases, OSM-MISO gradually exhibits a clear performance advantage, especially for small K . To achieve 10^{-2} SEP with $B = 6$ bits, OSM requires approximately 2.42 dB and 1.63 dB less power consumption than COAS-SM for $K = 2$ and

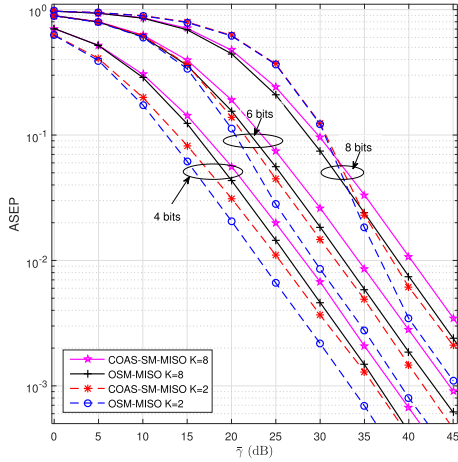


Fig. 7. SEP of COAS-SM-MISO and OSM-MISO for $N_t = 16$ and $B = 4, 6, 8$ bits.

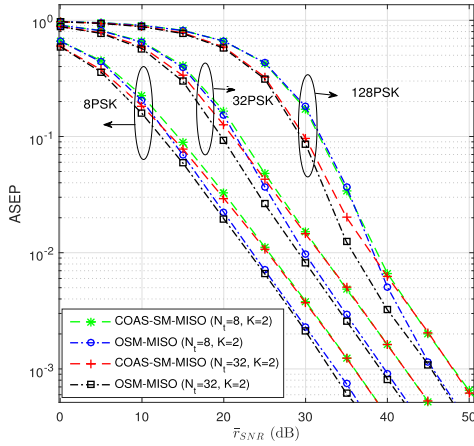


Fig. 8. Comparison of the COAS-SM-MISO and OSM-MISO for $N_t = 8$ and $N_t = 32$ with $B = 4, 6, 8$ bits, respectively.

$K = 8$, respectively. As shown in Fig. 7, at high SNR, despite having the same diversity order one, the OSM coding gain exceeds that of COAS-SM. For example, for $B = 6$ bits, $K = 2$ and $\bar{\gamma} = 30$ dB, OSM achieves approximately 42% SEP performance enhancement over COAS-SM. These results confirm energy efficiency and coding gain advantages of OSM-MISO over COAS-SM-MISO.

Fig. 8 illustrates the comparison between COAS-SM-MISO and OSM-MISO for $N_t = 8$ and $N_t = 32$ with $B = 4, 6, 8$ bits, respectively. Unlike Fig. 7, Fig. 8 studies the impact of using different antenna number N_t , with fixed $K = 2$. As we can observe from Fig. 8, for either COAS-SM-MISO or OSM-MISO, the benefit of increasing N_t becomes more prominent as the data rate B rises, especially at low-to-moderate SNR (the range is constantly expanding). And similar to Fig. 7, for any given N_t , the coding gain of OSM-MISO is significantly larger than COAS-SM-MISO, although such gap does not change much as N_t increases. Thus, OSM-MISO seems a better option than COAS-SM-MISO for high rate and low-complexity MIMO implementations such as massive MIMO or large-scale antenna systems [28].

In Fig. 9, OSM-MISO-BCS is compared with EDAS-SM-MISO-BCS for $N_t = 16$. Due to the high-complexity of

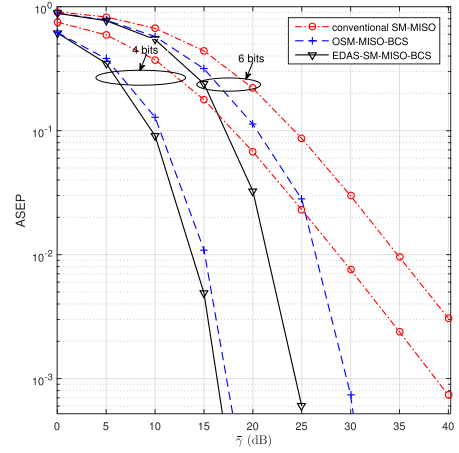


Fig. 9. SEP of conventional SM-MISO, EDAS-SM-MISO with BCS and OSM-MISO with BCS for $N_t = 16$ and $B = 4, 6$ bits.

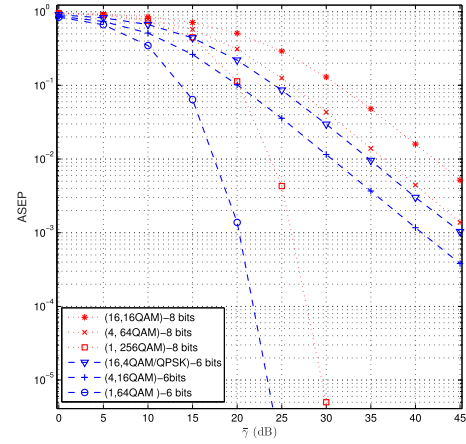


Fig. 10. Average SEP of OSM-MISO with QAM for $N_t = 16$ and $B = 6, 8$ bits.

computing EDAS-SM-MISO-BCS results, we only plot 4 and 6 bits data rate cases. Fig. 9 shows that, for 4 bits, there is a very small gap between the two schemes; and for 6 bits, OSM-MISO-BCS reduces more than half of the performance gap between EDAS-SM-MISO-BCS and conventional SM schemes. Therefore, our OSM-MISO scheme offers a useful performance-complexity trade-off.

D. Extension to OSM-MISO With QAM Scheme and OSM-MIMO Case

Fig. 10 depicts the SEP performance of OSM-MISO with M-QAM modulation for $N_t = 16$ and $B = 6, 8$ bits, respectively. We consider three possible combinations of (K, M) for each given B , i.e., $(K, M) = \{(1, 64QAM), (4, 16QAM), (16, 4QAM)\}$ for 6 bits and $(K, M) = \{(1, 256QAM), (4, 64QAM), (16, 16QAM)\}$ for 8 bits. As we can observe from Fig. 10, the curves of $(4, 16QAM)$, $(4, 64QAM)$ and $(16, 16QAM)$ have the same slope as the $(16, 4QAM)$ case, whose diversity order is only one due to the fact that $(16, 4QAM)$ is the same as $(16, QPSK)$. For any $(K, M) = (1, 2^B QAM)$, transmit diversity is achieved. These results agree with Section III-D

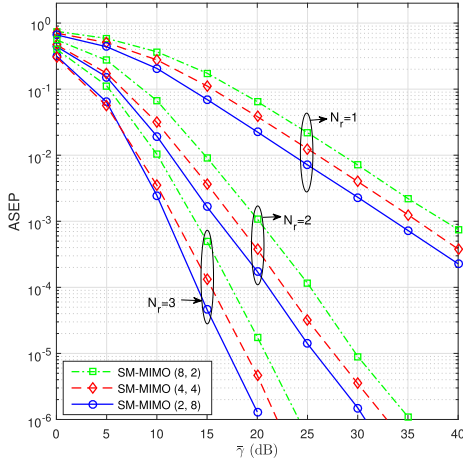


Fig. 11. SEP of OSM-MIMO for $N_t = 8$ and $B = 4$ bits.

that OSM-MISO with QAM achieves full-diversity order for $(K, M) = (1, 2^B QAM)$, but only offers diversity order one for all other (K, M) pairs. Although having the same diversity order, the SEP of OSM-MISO with M-QAM is substantially improved as K decreases. For example, the performance of (4, 16QAM) is better than (16, 4QAM) for $B = 6$ bits; and (4, 64QAM) outperforms (16, 16QAM) for $B = 8$ bits.

Although the MISO model (Fig. 1) formed the starting point of analyzing performance of the proposed OSM, one can easily extend the idea of OSM to MIMO (multiple antennas receiver $N_r \geq 1$), i.e., OSM-MIMO. Fig. 11 illustrates the SEP of OSM-MIMO with M-PSK for $N_t = 8$ and $B = 4$ bits (Monte Carlo simulations), and studies the impact of receiver diversity when receive antennas increase from 1 to 3. Section III.B showed that the diversity order of OSM-MISO with $1 < K \leq N_t$, i.e., $(K, M) = \{(8, 2), (4, 4), (2, 8)\}$ for $B = 4$ bits case, is just one. We thus focus on the changes in the performance of these three (K, M) pairs as N_r increases. The important observation from Fig. 11 is that the introducing one extra receive antenna substantially reduces the SEP. The diversity gain significantly increases with N_r and the diversity order is obviously exceeds one when $N_r > 1$, which means OSM-MIMO is inherently able to exploit receiver diversity.

V. CONCLUSIONS

This paper has proposed a novel concept of OSM, which involves the division of N_t transmit antennas to K equal groups and the selection of the best antenna from each group, and spatial modulation is then performed on these K antennas. We have developed a comprehensive error performance analysis OSM-MISO with PSK modulation as well as its asymptotic error expressions. We extended the analysis to QAM and OSM-MIMO was also studied via simulation. The simulation results validate the analytical derivations and also show that for a given N_t and fixed data rate B , as SNR increases, we should gradually use fewer antenna groups and larger signal constellation size in order to obtain the optimal SEP performance. Further, optimized OSM-MISO saves significant power compared to conventional SM-MISO (e.g. 12 dB power savings for $N_t = 8$, $B = 4$ bits at an SEP of 10^{-2}).

Moreover, compared to COAS-SM and EDAS-SM, OSM-MISO shows an excellent performance-complexity trade-off.

Future works include: i) The analysis of OSM can be extended to MIMO systems either with a priori single-antenna selection or with other diversity combining techniques at the receiver; ii) The proposed OSM scheme may also be amalgamated with the concept of TPC [27] to boost the transmit diversity of OSM for any given K . iii) With the ability to maintain the potential benefits of multiple antennas, the proposed OSM design paradigm constitutes an attractive low-complexity yet energy-efficient option for the family of LS-MIMO systems [28], such as Massive MIMO. Thus, OSM may be extended to Massive MIMO multiuser uplink and downlink design; and iv) Performance analysis of our OSM scheme under more practical imperfect CSIR scenario [35].

APPENDIX

A. Proof of Proposition 1

According to [30, eq. (30)] and [31, eq. (5.66)], we can write P_{signal} in (5) as

$$\begin{aligned}
 P_{\text{signal}} &= \frac{N_g}{\pi} \int_0^{\pi - \frac{\pi}{M}} \int_0^\infty e^{-z_k \left(\frac{\bar{\gamma} \sin^2(\frac{\pi}{M})}{\sin^2(\theta)} + 1 \right)} (1 - e^{-z_k})^{N_g - 1} dz_k d\theta \\
 &\stackrel{(a)}{=} \sum_{n=0}^{N_g - 1} \frac{\frac{1}{\pi} N_g! (-1)^n \int_0^{\pi - \frac{\pi}{M}} \int_0^\infty e^{-z_k \left(\frac{\bar{\gamma} \sin^2(\frac{\pi}{M})}{\sin^2(\theta)} + 1 + n \right)} dz_k d\theta}{n! (N_g - 1 - n)!} \\
 &= \sum_{n=0}^{N_g - 1} \frac{N_g! (-1)^n}{n! (N_g - 1 - n)!} \frac{1}{\pi} \int_0^{\pi - \frac{\pi}{M}} \frac{1}{\frac{\bar{\gamma} \sin^2(\frac{\pi}{M})}{\sin^2(\theta)} + 1 + n} d\theta \\
 &= \sum_{n=0}^{N_g - 1} \binom{N_g}{n+1} (-1)^n \frac{1}{\pi} \int_0^{\pi - \frac{\pi}{M}} \frac{\sin^2(\theta)}{\frac{\bar{\gamma} \sin^2(\frac{\pi}{M})}{1+n} + \sin^2(\theta)} d\theta, \tag{25}
 \end{aligned}$$

where (a) follows via the binomial expansion. By applying [31, eq. (5A.15)], we get the exact P_{signal} expression as in (9).

B. Proof of Lemma 1

Let $h_i = b_i e^{j\phi_i}$, $\forall i = 1, \dots, N_t$, where $b_i = |h_i|$ is the magnitude of h_i and ϕ_i is the phase. Since $h_i \sim \mathcal{CN}(0, 1)$, b_i follows the Rayleigh distribution as $f_{b_i}(u) = 2ue^{-u^2}$, and b_i^2 follows the exponential distribution as $f_{b_i^2}(v) = e^{-v}$. The phase ϕ_i is uniformly distributed over the range $[0, 2\pi]$, i.e., $f_{\phi_i}(t) = \frac{1}{2\pi}$, and it is independent of b_i . For Group k , $\forall k = 1, \dots, K$, as $N_{(k)} = \arg \max_{k(N_g - 1) + 1 \leq i \leq kN_g} b_i^2$, the joint cumulative distribution function (CDF) of the magnitude and phase of $g_{(k)}$ is given as

$$\begin{aligned}
 F_{(r_k, \theta_k)}(x, y) &= \Pr \left\{ b_{N_{(k)}} \leq x, \phi_{N_{(k)}} \leq y \mid b_{N_{(k)}}^2 = \max_{k(N_g - 1) + 1 \leq i \leq kN_g} b_i^2 \right\} \\
 &= \frac{\Pr \left\{ b_{N_{(k)}} \leq x, \phi_{N_{(k)}} \leq y, b_{N_{(k)}}^2 = \max_{k(N_g - 1) + 1 \leq i \leq kN_g} b_i^2 \right\}}{\Pr \left\{ b_{N_{(k)}}^2 = \max_{i=k(N_g - 1) + 1}^{kN_g} b_i^2 \right\}}
 \end{aligned}$$

$$\begin{aligned}
&= \frac{\left(\int_0^y \frac{dt}{2\pi}\right) \int_0^x \left(\int_0^{u^2} e^{-v} dv\right)^{N_g-1} 2ue^{-u^2} du}{\int_0^\infty \left(\int_0^{u^2} e^{-v} dv\right)^{N_g-1} 2ue^{-u^2} du} \\
&= \frac{y}{2\pi} \left(1 - e^{-x^2}\right)^{N_g}. \tag{26}
\end{aligned}$$

Thus, the CDF of r_k is given as $F_{r_k}(x) = F_{(r_k, \theta_k)}(x, 2\pi) = (1 - e^{-x^2})^{N_g}$ and the CDF of θ_k is given as $F_{\theta_k}(y) = F_{(r_k, \theta_k)}(\infty, y) = \frac{y}{2\pi}$. Since we have $F_{(r_k, \theta_k)}(x, y) = F_{r_k}(x)F_{\theta_k}(y)$, random variables r_k and θ_k are independent. The PDFs of r_k and θ_k can be obtained respectively as

$$\begin{aligned}
f_{r_k}(x) &= \frac{\partial F_{r_k}(x)}{\partial x} = 2N_g \left(1 - e^{-x^2}\right)^{N_g-1} x e^{-x^2}, \\
f_{\theta_k}(y) &= \frac{\partial F_{\theta_k}(y)}{\partial y} = \frac{1}{2\pi}. \tag{27}
\end{aligned}$$

C. Proof of Lemma 2

As r_k and $r_{k'}$ are i.i.d. with the pdf given in Lemma 1, we have,

$$\begin{aligned}
\Lambda(\rho) &= (\mathbb{E}_{r_k} [J_0(r_k \rho)])^2 \\
&= \left(\int_0^\infty J_0(r_k \rho) 2N_g \left(1 - e^{-r_k^2}\right)^{N_g-1} r_k e^{-r_k^2} dr_k \right)^2 \\
&\stackrel{\text{let } t \triangleq r_k^2}{=} \left(N_g \int_0^\infty J_0(\sqrt{t} \rho) \left(1 - e^{-t}\right)^{N_g-1} e^{-t} dt \right)^2 \\
&\stackrel{(a)}{=} \left(\sum_{n=0}^{N_g-1} \frac{N_g! (-1)^n}{n! (N_g - 1 - n)!} \int_0^\infty J_0(\sqrt{t} \rho) e^{-(n+1)t} dt \right)^2 \\
&\stackrel{(b)}{=} \left(\sum_{n=0}^{N_g-1} \frac{N_g! (-1)^n}{(n+1)! (N_g - 1 - n)!} e^{-\frac{\rho^2}{4(n+1)}} \right)^2 \\
&= \sum_{n=0}^{N_g-1} \sum_{l=0}^{N_g-1} \frac{(N_g!)^2 (-1)^{n+l} e^{-\frac{n+l+2}{4(n+1)(l+1)} \rho^2}}{(n+1)! (N_g - 1 - n)! (l+1)! (N_g - 1 - l)!} \tag{28}
\end{aligned}$$

where (a) is obtained by applying the Binomial theorem $(1+x)^n = \sum_{i=0}^n \frac{n!}{i!(n-i)!} x^i$ and (b) is due to $\int_0^\infty J_0(b\sqrt{x}) e^{-ax} dx = \frac{1}{a} e^{-\frac{b^2}{4a}}$ [36, eq. (6.614)]. Substituting (28) into (12), we have,

$$\begin{aligned}
f_\Psi(x) &= x \int_0^\infty \rho J_0(x\rho) \Lambda(\rho) d\rho \\
&= \sum_{n=0}^{N_g-1} \sum_{l=0}^{N_g-1} \frac{(N_g!)^2 (-1)^{n+l} x \int_0^\infty \rho J_0(x\rho) e^{-\frac{n+l+2}{4(n+1)(l+1)} \rho^2} d\rho}{(n+1)! (N_g - 1 - n)! (l+1)! (N_g - 1 - l)!} \\
&\stackrel{(c)}{=} \sum_{n=0}^{N_g-1} \sum_{l=0}^{N_g-1} \frac{2(N_g!)^2 (-1)^{n+l} x e^{-\frac{(n+1)(l+1)}{n+l+2} x^2}}{n! (N_g - 1 - n)! (N_g - 1 - l)! (n+l+2)} \tag{29}
\end{aligned}$$

where (c) is due to changing variable ρ to ρ^2 and then applying [36, eq. (6.614)].

D. Proof of Proposition 3

(25) can be rewritten as,

$$\begin{aligned}
P_{\text{signal}} &= \sum_{n=0}^{N_g-1} \binom{N_g}{n+1} (-1)^n \frac{1}{\pi} \int_0^{\pi - \frac{\pi}{M}} \frac{(1+n) \sin^2(\theta)}{\bar{\gamma} \sin^2\left(\frac{\pi}{M}\right)} \\
&\quad \times \left(1 + \frac{(1+n) \sin^2(\theta)}{\bar{\gamma} \sin^2\left(\frac{\pi}{M}\right)}\right)^{-1} d\theta. \tag{30}
\end{aligned}$$

At high SNR ($\bar{\gamma} \rightarrow \infty$), we have $\frac{(1+n) \sin^2(\theta)}{\bar{\gamma} \sin^2\left(\frac{\pi}{M}\right)} \rightarrow 0$. Thus by applying the Binomial expansion $(1+x)^{-1} = \sum_{i=0}^\infty (-1)^i x^i$ for $|x| < 1$, we find

$$\left(1 + \frac{(1+n) \sin^2(\theta)}{\bar{\gamma} \sin^2\left(\frac{\pi}{M}\right)}\right)^{-1} = \sum_{i=0}^\infty (-1)^i \left(\frac{(1+n) \sin^2(\theta)}{\bar{\gamma} \sin^2\left(\frac{\pi}{M}\right)}\right)^i. \tag{31}$$

Substituting (31) into (30), we find (32), as shown at the top of the next page, where in (a), $D_i \triangleq \frac{1}{\pi} \int_0^{\pi - \frac{\pi}{M}} \sin^{2(i+1)}(\theta) d\theta = \frac{1}{2\sqrt{\pi}} \frac{\Gamma(i + \frac{3}{2})}{(i+1)!} + \frac{1}{\pi} \cos\left(\frac{\pi}{M}\right) {}_2F_1\left(\frac{1}{2}, -i - \frac{1}{2}; \frac{3}{2}; \cos^2\left(\frac{\pi}{M}\right)\right)$, with ${}_2F_1(a, b; c; z)$ being a Gauss hypergeometric function. According to [37, Corollary 2] and [38, Proposition 2.1], we can acquire $\sum_{n=1}^{N_g} \binom{N_g}{n} (-1)^n n^{i+1} = 0$, $\forall i < N_g - 1$, which leads to

$$J_1 = 0. \tag{33}$$

From [37, Th. 1], we deduce that $\sum_{n=1}^{N_g} \binom{N_g}{n} (-1)^n n^{N_g} = (-1)^{N_g} N_g!$, which results in,

$$\begin{aligned}
J_2 &= -(-1)^{N_g-1} \left(\frac{1}{\bar{\gamma} \sin^2\left(\frac{\pi}{M}\right)}\right)^{N_g} D_{N_g-1} (-1)^{N_g} N_g! \\
&= N_g! \sin^{-2N_g} \left(\frac{\pi}{M}\right) D_{N_g-1} \bar{\gamma}^{-N_g}. \tag{34}
\end{aligned}$$

It is easy to verify that $\lim_{\bar{\gamma} \rightarrow \infty} \frac{J_3}{(\bar{\gamma})^{-N_g}} = 0$, which implies that at high SNR ($\bar{\gamma} \rightarrow \infty$), J_3 can be written as

$$J_3 = \mathcal{O}(\bar{\gamma}^{-N_g-1}). \tag{35}$$

Therefore, by substituting (33)-(35) back into (32), we have, at high SNR, P_{signal} can be asymptotically formulated as,

$$\begin{aligned}
P_{\text{signal}} &= N_g! \sin^{-2N_g} \left(\frac{\pi}{M}\right) \left[\frac{1}{2\sqrt{\pi}} \frac{\Gamma(N_g + \frac{1}{2})}{N_g!} \right. \\
&\quad \left. + \frac{1}{\pi} \cos\left(\frac{\pi}{M}\right) {}_2F_1\left(\frac{1}{2}, \frac{1}{2} - N_g; \frac{3}{2}; \cos^2\left(\frac{\pi}{M}\right)\right) \right] \\
&\quad \times \bar{\gamma}^{-N_g} + \mathcal{O}(\bar{\gamma}^{-N_g-1}). \tag{36}
\end{aligned}$$

E. Proof of Proposition 4

Let $Y \triangleq \Psi^2 = |g_{(k)} s_m - g_{(k')} s_{m'}|^2$. Then from the definition in (7), $\overline{\text{APEP}}$ can be written as

$$\overline{\text{APEP}} = \int_0^\infty Q\left(\sqrt{\frac{\bar{\gamma} y}{2}}\right) f_Y(y) dy. \tag{37}$$

According to [34], [39], and [40], $\overline{\text{APEP}}$ at high SNR depends mainly on the behavior of $f_Y(y)$ at $y \rightarrow 0^+$. More specifically,

$$\begin{aligned}
P_{\text{signal}} &= \sum_{n=0}^{N_g-1} \binom{N_g}{n+1} (-1)^n \frac{1}{\pi} \int_0^{\pi-\frac{\pi}{M}} \sum_{i=0}^{\infty} (-1)^i \left(\frac{(1+n) \sin^2(\theta)}{\bar{\gamma} \sin^2\left(\frac{\pi}{M}\right)} \right)^{i+1} d\theta, \\
&= \sum_{i=0}^{\infty} (-1)^i \left(\frac{1}{\bar{\gamma} \sin^2\left(\frac{\pi}{M}\right)} \right)^{i+1} \left[\frac{1}{\pi} \int_0^{\pi-\frac{\pi}{M}} (\sin(\theta))^{2(i+1)} d\theta \right] \sum_{n=0}^{N_g-1} \binom{N_g}{n+1} (-1)^n (1+n)^{i+1} \\
&\stackrel{(a)}{=} - \sum_{i=0}^{\infty} (-1)^i \left(\frac{1}{\bar{\gamma} \sin^2\left(\frac{\pi}{M}\right)} \right)^{i+1} D_i \sum_{n=1}^{N_g} \binom{N_g}{n} (-1)^n n^{i+1} \\
&= - \underbrace{\sum_{i=0}^{N_g-2} (-1)^i \left(\frac{1}{\bar{\gamma} \sin^2\left(\frac{\pi}{M}\right)} \right)^{i+1} D_i \sum_{n=1}^{N_g} \binom{N_g}{n} (-1)^n n^{i+1}}_{\triangleq J_1} \\
&\quad \times \underbrace{-(-1)^{N_g-1} \left(\frac{1}{\bar{\gamma} \sin^2\left(\frac{\pi}{M}\right)} \right)^{N_g} D_{N_g-1} \sum_{n=1}^{N_g} \binom{N_g}{n} (-1)^n n^{N_g}}_{\triangleq J_2} \\
&\quad \times \underbrace{- \sum_{i=N_g}^{\infty} (-1)^i \left(\frac{1}{\bar{\gamma} \sin^2\left(\frac{\pi}{M}\right)} \right)^{i+1} D_i \sum_{n=1}^{N_g} \binom{N_g}{n} (-1)^n n^{i+1}}_{\triangleq J_3} \tag{32}
\end{aligned}$$

assume $f_Y(y)$ can be written as $f_Y(y) = ay^t + \mathcal{O}(y^t)$, $a > 0$ at $y \rightarrow 0^+$, then at high SNR, $\overline{\text{APEP}}$ can be formulated as [34], [39], [40],

$$\overline{\text{APEP}} = \frac{2^t a \Gamma(t + \frac{3}{2})}{\sqrt{\pi}(t+1)} \left(\frac{1}{2} \bar{\gamma} \right)^{-(t+1)} + \mathcal{O}(\bar{\gamma}^{-(t+2)}). \tag{38}$$

Thus, we just need to find the unknown t and a . From Lemma 2, it is easy to obtain

$$\begin{aligned}
f_Y(y) &= \frac{1}{2} \frac{1}{\sqrt{y}} f_{\Psi}(\sqrt{y}) \\
&= \sum_{n=0}^{N_g-1} \sum_{l=0}^{N_g-1} \frac{(N_g!)^2 (-1)^{n+l} e^{-\frac{y(n+1)(l+1)}{n+l+2}}}{n!(N_g-1-n)!l!(N_g-1-l)!(n+l+2)} \\
&= \sum_{n=0}^{N_g-1} \sum_{l=0}^{N_g-1} \frac{(N_g!)^2 (-1)^{n+l}}{n!(N_g-1-n)!l!(N_g-1-l)!(n+l+2)} \\
&\quad \times \sum_{i=0}^{\infty} \frac{(-1)^i}{i!} \left(\frac{(n+1)(l+1)}{n+l+2} \right)^i y^i \tag{39}
\end{aligned}$$

where the last equality is obtained by utilizing the Taylor series expansion of the exponential function. From (39), we have

$$\begin{aligned}
a &= \sum_{n=0}^{N_g-1} \sum_{l=0}^{N_g-1} \frac{(N_g!)^2 (-1)^{n+l}}{n!(N_g-1-n)!l!(N_g-1-l)!(n+l+2)}, \\
&= \sum_{n=0}^{N_g-1} \sum_{l=0}^{N_g-1} \binom{N_g}{n+1} \binom{N_g}{l+1} \frac{(-1)^{n+l} (n+1)(l+1)}{n+l+2} \\
&= - \sum_{n=0}^{N_g-1} \sum_{l=0}^{N_g-1} (n+1)(l+1) \binom{N_g}{n+1} \binom{N_g}{l+1} \int_{-1}^0 x^{n+l+1} dx
\end{aligned}$$

$$\begin{aligned}
&= - \int_{-1}^0 x \left(\sum_{n=0}^{N_g-1} (n+1) \binom{N_g}{n+1} x^n \right)^2 dx \\
&= - \int_{-1}^0 x \left(\frac{d}{dx} \sum_{n=0}^{N_g} \binom{N_g}{n} x^n \right)^2 dx, \tag{40}
\end{aligned}$$

which yields,

$$\begin{aligned}
a &= - \int_{-1}^0 x \left(\frac{d}{dx} (1+x)^{N_g} \right)^2 dx \\
&= - \int_{-1}^0 N_g^2 x (1+x)^{2N_g-2} dx \\
&= \frac{N_g}{4N_g-2}. \tag{41}
\end{aligned}$$

Thus a is only depends on N_g , and

$$t = 0. \tag{42}$$

By substituting (41) and (42) into (38), we can obtain,

$$\overline{\text{APEP}} = \frac{N_g}{4N_g-2} \bar{\gamma}^{-1} + \mathcal{O}(\bar{\gamma}^{-2}), \quad \bar{\gamma} \gg 1. \tag{43}$$

REFERENCES

- [1] Y. A. Chau and S.-H. Yu, "Space modulation on wireless fading channels," in *Proc. IEEE VTS 54th Veh. Technol. Conf. (VTC Fall)*, vol. 3, Oct. 2001, pp. 1668–1671.
- [2] M. Di Renzo, H. Haas, A. Ghayeb, S. Sugiura, and L. Hanzo, "Spatial modulation for generalized MIMO: Challenges, opportunities, and implementation," *Proc. IEEE*, vol. 102, no. 1, pp. 56–103, Jan. 2014.
- [3] R. Rajashekar, K. V. S. Hari, and L. Hanzo, "Reduced-complexity ML detection and capacity-optimized training for spatial modulation systems," *IEEE Trans. Commun.*, vol. 62, no. 1, pp. 112–125, Jan. 2014.

- [4] H. Men and M. Jin, "A low-complexity ML detection algorithm for spatial modulation systems with MPSK constellation," *IEEE Commun. Lett.*, vol. 18, no. 8, pp. 1375–1378, Aug. 2014.
- [5] Z. Pi and F. Khan, "An introduction to millimeter-wave mobile broadband systems," *IEEE Commun. Mag.*, vol. 49, no. 6, pp. 101–107, Jun. 2011.
- [6] P. Liu, M. Di Renzo, and A. Springer, "Line-of-sight spatial modulation for indoor mmWave communication at 60 GHz," *IEEE Trans. Wireless Commun.*, vol. 15, no. 11, pp. 7373–7389, Nov. 2016.
- [7] N. S. Perovic, P. Liu, M. Di Renzo, and A. Springer, "Receive spatial modulation for LOS mmWave communications based on TX beamforming," *IEEE Commun. Lett.*, vol. 21, no. 4, pp. 921–924, Apr. 2017.
- [8] P. Liu, J. Blumenstein, N. S. Perović, M. D. Renzo, and A. Springer, "Performance of generalized spatial modulation MIMO over measured 60 GHz indoor channels," *IEEE Trans. Commun.*, vol. 66, no. 1, pp. 133–148, Jan. 2018.
- [9] N. Serafimovski *et al.*, "Practical implementation of spatial modulation," *IEEE Trans. Veh. Technol.*, vol. 62, no. 9, pp. 4511–4523, Nov. 2013.
- [10] P. Yang, M. Di Renzo, Y. Xiao, S. Li, and L. Hanzo, "Design guidelines for spatial modulation," *IEEE Commun. Surveys Tuts.*, vol. 17, no. 1, pp. 6–26, 1st Quart., 2015.
- [11] A. Stavridis, S. Sinanovic, M. Di Renzo, and H. Haas, "Energy evaluation of spatial modulation at a multi-antenna base station," in *Proc. IEEE 78th Veh. Technol. Conf. (VTC Fall)*, Las Vegas, NV, USA, Sep. 2013, pp. 1–5.
- [12] M. Di Renzo and H. Haas, "On transmit diversity for spatial modulation MIMO: Impact of spatial constellation diagram and shaping filters at the transmitter," *IEEE Trans. Veh. Technol.*, vol. 62, no. 6, pp. 2507–2531, Jul. 2013.
- [13] W.-H. Chung and C.-Y. Hung, "Multi-antenna selection using space shift keying in MIMO systems," in *Proc. IEEE Veh. Technol. Conf. (VTC)*, May 2012, pp. 1–5.
- [14] R. Rajashekar, K. V. S. Hari, and L. Hanzo, "Antenna selection in spatial modulation systems," *IEEE Commun. Lett.*, vol. 17, no. 3, pp. 521–524, Mar. 2013.
- [15] Z. Zhou, N. Ge, and X. Lin, "Reduced-complexity antenna selection schemes in spatial modulation," *IEEE Commun. Lett.*, vol. 18, no. 1, pp. 14–17, Jan. 2014.
- [16] R. Rajashekar, K. V. S. Hari, and L. Hanzo, "Quantifying the transmit diversity order of euclidean distance based antenna selection in spatial modulation," *IEEE Signal Process. Lett.*, vol. 22, no. 9, pp. 1434–1437, Sep. 2015.
- [17] N. Pillay and H. Xu, "Comments on 'Antenna selection in spatial modulation systems,'" *IEEE Commun. Lett.*, vol. 17, no. 9, pp. 1681–1683, Sep. 2013.
- [18] K. Ntontin, M. Di Renzo, A. I. Perez-Neira, and C. Verikoukis, "A low-complexity method for antenna selection in spatial modulation systems," *IEEE Commun. Lett.*, vol. 17, no. 12, pp. 2312–2315, Dec. 2013.
- [19] M. Maleki, H. R. Bahrami, and A. Alizadeh, "Adaptive antenna subset selection and constellation breakdown for spatial modulation," *IEEE Commun. Lett.*, vol. 18, no. 9, pp. 1649–1652, Sep. 2014.
- [20] N. Wang, W. Liu, H. Men, M. Jin, and H. Xu, "Further complexity reduction using rotational symmetry for EDAS in spatial modulation," *IEEE Commun. Lett.*, vol. 18, no. 10, pp. 1835–1838, Oct. 2014.
- [21] J. Zheng and J. Chen, "Further complexity reduction for antenna selection in spatial modulation systems," *IEEE Commun. Lett.*, vol. 19, no. 6, pp. 937–940, Jun. 2015.
- [22] Z. Sun, Y. Xiao, L. You, L. Yin, P. Yang, and S. Li, "Cross-entropy-based antenna selection for spatial modulation," *IEEE Commun. Lett.*, vol. 20, no. 3, pp. 622–625, Mar. 2016.
- [23] P. Yang, Y. Xiao, Y. L. Guan, S. Li, and L. Hanzo, "Transmit antenna selection for multiple-input multiple-output spatial modulation systems," *IEEE Trans. Commun.*, vol. 64, no. 5, pp. 2035–2048, May 2016.
- [24] Z. Sun, Y. Xiao, P. Yang, S. Li, and W. Xiang, "Transmit antenna selection schemes for spatial modulation systems: Search complexity reduction and large-scale MIMO applications," *IEEE Trans. Veh. Technol.*, vol. 66, no. 9, pp. 8010–8021, Sep. 2017.
- [25] R. Rajashekar, K. V. S. Hari, and L. Hanzo, "Transmit antenna subset selection in spatial modulation relying on a realistic error-infested feedback channel," *IEEE Access*, vol. 6, pp. 5879–5890, 2017.
- [26] R. Rajashekar, M. Di Renzo, K. C. S. Hari, and L. Hanzo, "A generalized transmit and receive diversity condition for feedback-assisted MIMO systems: Theory and applications in full-duplex spatial modulation," *IEEE Trans. Signal Process.*, vol. 65, no. 24, pp. 6505–6519, Dec. 2017.
- [27] P. Yang, Y. L. Guan, Y. Xiao, M. Di Renzo, S. Li, and L. Hanzo, "Transmit precoded spatial modulation: Maximizing the minimum Euclidean distance versus minimizing the bit error ratio," *IEEE Trans. Wireless Commun.*, vol. 15, no. 3, pp. 2054–2068, Mar. 2016.
- [28] P. Yang *et al.*, "Single-carrier SM-MIMO: A promising design for broadband large-scale antenna systems," *IEEE Commun. Surveys Tuts.*, vol. 18, no. 3, pp. 1687–1716, 3rd Quart., 2016.
- [29] M. Di Renzo and H. Haas, "Bit error probability of SM-MIMO over generalized fading channels," *IEEE Trans. Veh. Technol.*, vol. 61, no. 3, pp. 1124–1144, Mar. 2012.
- [30] Z. Chen, Z. Chi, Y. Li, and B. Vucetic, "Error performance of maximal-ratio combining with transmit antenna selection in flat Nakagami-m fading channels," *IEEE Trans. Wireless Commun.*, vol. 8, no. 1, pp. 424–431, Jan. 2009.
- [31] M. K. Simon and M.-S. Alouini, *Digital Communication Over Fading Channels: A Unified Approach to Performance Analysis*. New York, NY, USA: Wiley, 2000.
- [32] H. A. David and H. N. Nagaraja, *Order Statistics* (Wiley Series in Probability and Statistics), 3rd ed. Hoboken, NJ, USA: Wiley, 2005.
- [33] A. Abdi, H. Hashemi, and S. Nader-Esfahani, "On the PDF of the sum of random vectors," *IEEE Trans. Commun.*, vol. 48, no. 1, pp. 7–12, Jan. 2000.
- [34] Z. Wang and G. B. Giannakis, "A simple and general parameterization quantifying performance in fading channels," *IEEE Trans. Commun.*, vol. 51, no. 8, pp. 1389–1398, Aug. 2003.
- [35] R. Rajashekar, K. V. S. Hari, K. Giridhar, and L. Hanzo, "Performance analysis of antenna selection algorithms in spatial modulation systems with imperfect CSIR," in *Proc. 19th Eur. Wireless Conf. (EW)*, Guildford, U.K., Apr. 2013, pp. 1–5.
- [36] D. Zwillinger, *Table of Integrals, Series, and Products*, 8th ed. New York, NY, USA: Elsevier, 2014.
- [37] S. M. Ruiz, "An algebraic identity leading to Wilson's theorem," *Math. Gazette*, vol. 80, no. 489, pp. 579–582, Nov. 1996.
- [38] R. Garrappa, "Some formulas for sums of binomial coefficients and gamma functions," *Int. Math. Forum*, vol. 2, no. 15, pp. 725–733, 2007.
- [39] Y. Dhungana and C. Tellambura, "New simple approximations for error probability and outage in fading," *IEEE Commun. Lett.*, vol. 16, no. 11, pp. 1760–1763, Nov. 2012.
- [40] Y. Dhungana and C. Tellambura, "Uniform approximations for wireless performance in fading channels," *IEEE Trans. Commun.*, vol. 61, no. 11, pp. 4768–4779, Nov. 2013.



Yuanyuan He (S'08–M'12) received the Ph.D. degree from the Department of Electrical and Electronic Engineering, The University of Melbourne, Melbourne, VIC, Australia. She is currently a Research Fellow with The University of Melbourne. In 2017, she was a Visiting Researcher with the Department of Electrical and Computer Engineering, University of Alberta, Edmonton, AB, Canada. Her current research interests include the area of wireless communications, including resource allocation, spatial modulation, and full duplex communications.



Saman Atapattu (M'14) received the B.Sc. degree in electrical and electronics engineering from the University of Peradeniya, Sri Lanka, the M.Eng. degree in telecommunications from the Asian Institute of Technology, Thailand, and the Ph.D. degree in electrical engineering from the University of Alberta, Edmonton, AB, Canada. He is currently a Research Fellow with the Department of Electrical and Electronic Engineering, The University of Melbourne, Melbourne, VIC, Australia. His general research interests include wireless communications and signal processing.



Chintha Tellambura (F'11) received the B.Sc. degree (Hons.) from the University of Moratuwa, Sri Lanka, the M.Sc. degree in electronics from King's College, University of London, U.K., and the Ph.D. degree in electrical engineering from the University of Victoria, Victoria, BC, Canada.

He was with Monash University, Clayton, VIC, Australia, from 1997 to 2002. He is currently a Professor with the Department of Electrical and Computer Engineering, University of Alberta. His current research interests include the design, modeling, and analysis of cognitive radio, heterogeneous cellular networks, 5G wireless networks, and machine learning algorithms.

He has authored or co-authored over 500 journal and conference papers with an h-index of 66 from Google Scholar. He received best paper awards from the Communication Theory Symposium in the 2012 IEEE International Conference on Communications (ICC), Canada, and the 2017 ICC, France.

He is the winner of the prestigious McCalla Professorship and the Killam Annual Professorship from the University of Alberta. In 2011, he was elected as an IEEE Fellow for his contributions to physical layer wireless communication theory. In 2017, he was elected as a fellow of the Canadian Academy of Engineering. He served as an Editor for the IEEE TRANSACTIONS ON COMMUNICATIONS from 1999 to 2011 and the IEEE TRANSACTIONS ON WIRELESS COMMUNICATIONS from 2001 to 2007. He was the Area Editor of the *Wireless Communications Systems and Theory* from 2007 to 2012.



Jamie S. Evans (S'93–M'98–SM'17) was born in Newcastle, NSW, Australia, in 1970. He received the B.S. degree in physics and the B.E. degree in computer engineering from the University of Newcastle in 1992 and 1993, respectively, and the M.S. and Ph.D. degrees in electrical engineering from The University of Melbourne, Australia, in 1996 and 1998, respectively. From 1998 to 1999, he was a Visiting Researcher with the Department of Electrical Engineering and Computer Science, University of California at Berkeley, Berkeley, CA, USA. Since returning to Australia in 1999, he has held academic positions at The University of Sydney, The University of Melbourne, and Monash University. He is currently a Professor and the Deputy Dean of the Melbourne School of Engineering, The University of Melbourne. His research interests include communications theory, information theory, and statistical signal processing with a focus on wireless communications networks. He received the University Medal upon graduation from the University of Newcastle. He was awarded the Chancellor's Prize for excellence for his Ph.D. thesis.